Available online at www.sciencedirect.com
ScienceDirect
Journal of Computational Physics 227 (2008) 3921–3939
JOURNAL OF COMPUTATIONAL PHYSICS
www.elsevier.com/locate/jcp

A numerical study of three-dimensional liquid sloshing in tanks

Dongming Liu [a], Pengzhi Lin [b,*]

[a] Department of Civil Engineering, National University of Singapore, Kent Ridge Crescent, Singapore 119077, Singapore
[b] State Key Laboratory of Hydraulics and Mountain River Engineering, Sichuan University, Chengdu, Sichuan 610065, China

Received 16 July 2007; received in revised form 14 November 2007; accepted 3 December 2007
Available online 23 December 2007

Abstract

A numerical model NEWTANK (Numerical Wave TANK) has been developed to study three-dimensional (3-D) non-linear liquid sloshing with broken free surfaces. The numerical model solves the spatially averaged Navier–Stokes equations, which are constructed on a non-inertial reference frame having arbitrary six degree-of-freedom (DOF) of motions, for two-phase flows. The large-eddy-simulation (LES) approach is adopted to model the turbulence effect by using the Smagorinsky sub-grid scale (SGS) closure model. The two-step projection method is employed in the numerical solutions, aided by the Bi-CGSTAB technique to solve the pressure Poisson equation for the filtered pressure field. The second-order accurate volume-of-fluid (VOF) method is used to track the distorted and broken free surface. Laboratory experiments are conducted for both 2-D and 3-D non-linear liquid sloshing in a rectangular tank. A linear analytical solution of 3-D liquid sloshing under the coupled surge and sway excitation is also developed in this study. The numerical model is first validated against the available analytical solution and experimental data for 2-D liquid sloshing of both inviscid and viscous fluids. The validation is further extended to 3-D liquid sloshing. The numerical results match with the analytical solution when the excitation amplitude is small. When the excitation amplitude is large where sloshing becomes highly non-linear, large discrepancies are developed between the numerical results and the analytical solutions, the former of which, however, agree well with the experimental data. Finally, as a demonstration, a violent liquid sloshing with broken free surfaces under six DOF excitations is simulated and discussed.

Keywords: Liquid sloshing; Three-dimensional numerical model; Navier–Stokes equations; Non-inertial reference frame; VOF method; Broken free surface; Analytical solution

1. Introduction

Liquid sloshing is a kind of wave motion inside a partially filled tank. The sloshing phenomenon is of great theoretical and practical importance in coastal and offshore engineering with regard to the safety of sea transport of oil and liquefied natural gas (LNG). Under external excitations that are of large amplitude or near the

* Corresponding author. Tel.: +86 28 85406172; fax: +86 28 85405148.
E-mail addresses: liudongming@nus.edu.sg (D. Liu), cvelinpz@scu.edu.cn (P. Lin).

0021-9991/$ - see front matter © 2007 Elsevier Inc. All rights reserved.
doi:10.1016/j.jcp.2007.12.006

natural frequency of sloshing, the liquid inside a partially filled tank is prone to violent oscillations and large impact pressure on the tank. A comprehensive review of liquid sloshing can be found in [17,21].

Sloshing waves in a rectangular tank have been intensively studied in the last a few decades. Many researchers have devoted their efforts to study sloshing analytically based on potential flow theory. For example, Faltinsen [10] derived a linear analytical solution for liquid sloshing in a horizontally excited 2-D rectangular tank and this solution has been widely used in the validation of numerical models. Recently, Faltinsen et al. [11] and Faltinsen and Timokha [12] developed a multimodal approach to describe the non-linear sloshing in a rectangular tank with finite water depth. Later, Hill [16] analyzed the transient behavior of the resonated waves by relaxing many of the assumptions adopted in the previous studies. However, these theoretical analyses are not valid for viscous and turbulent flows, so the overturning and breaking waves during violent liquid sloshing cannot be described. On the other hand, laboratory measurements of wave height and hydrodynamic pressure have been reported by Verhagen and Wijingaarden [37], Okamoto and Kawahara [29], Okamoto and Kawahara [30], Akyildiz and Ünal [1], etc. These measurements are very useful for validating theoretical solution and numerical results.

Many numerical models solve Laplace equation for liquid sloshing based on potential flow theory. The earliest pioneer is Faltinsen [10], who developed the boundary element method (BEM) model to study the liquid sloshing problems and compared the numerical results with the linear analytical solution. Later, Nakayama and Washizu [28] adopted the same method to study liquid sloshing in an excited rectangular tank subjected to surge, heave, or pitch motion. Meanwhile, the finite element method (FEM) is another popular numerical method in solving Laplace equation. Nakayama and Washizu [27] analyzed the non-linear liquid sloshing in a 2-D rectangular tank under pitch excitation by using FEM. Their work was followed and refined by Cho and Lee [7], who analyzed the large amplitude sloshing in a 2-D tank. Wang and Khoo [33] studied 2-D non-linear sloshing problems under random excitations by using fully non-linear wave theory. Wu et al. [35] conducted a series of 3-D demonstrations on liquid sloshing based on FEM. Unfortunately, their 3-D numerical results were not compared to any experimental data. The finite difference method (FDM) is another means to solve Laplace equation. Coordinate transformations are usually used when Laplace equation is solved by FDM. For example, Chen et al. [3] adopted a curvilinear coordinate system to map the sloshing from the non-rectangular physical domain into a rectangular computational domain. Similar ideas have also been employed by Frandsen and Borthwick [13] and Frandsen [14], who conducted a series of numerical experiment in a 2-D tank which is moved both horizontally and vertically by using σ-coordinate transformation. However, because of the use of potential flow assumption, both viscous sloshing and rotational motion of the liquid cannot be captured by the models introduced above.

Alternatively, one can solve Navier–Stokes equations (NSE) or its kind for viscous liquid sloshing. For example, Armenio and La Rocca [2] adopted the FDM to solve the Reynolds Averaged Navier–Stokes (RANS) equations and compared the results to that from shallow water equations (SWE). They observed that, not surprisingly, the RANS model provides more accurate results than the SWE model. Meanwhile, some researchers have applied NSE to study 2-D liquid sloshing by using coordinate transformation, such as Chen and Chiang [4], Chen [5] and Chen and Nokes [6]. On the other hand, Kim [19] and Kim et al. [20] employed the SOLA scheme to study liquid sloshing in a 3-D container and adopted the concept of buffer zone to calculate the impact pressure on the tank ceiling. The height function was employed in their model to track the free surface that restricts the free surface to be single-valued and thus the model is not applicable to simulate broken free surface. So far, there has been no report for a 3-D model that can simulate viscous liquid sloshing in a tank with broken free surfaces.

In this study, we shall present a two-phase fluid flow model that solves the spatially averaged Navier–Stokes equations constructed in an arbitrarily moving non-inertial frame to represent a rigid tank under six degree-of-freedom (DOF) external excitation. The volume-of-fluid (VOF) method is adopted to track the free surface motion. The concept of piecewise linear interface calculation (PLIC) [15], which represents the free surface in each cell by an inclined plane, is employed in this 3-D model. The large-eddy-simulation (LES) is used for turbulence modeling. A linear analytical solution is proposed for 3-D liquid sloshing under combined surge and sway excitations. The model is validated by comparing the numerical results with the linear analytical solution, experimental data and other numerical solution for both 2-D and 3-D sloshing. Finally, a demonstration of violent liquid sloshing in a 3-D tank with broken free surfaces is presented.

2. Mathematical model

The motions of an incompressible fluid are governed by the spatially averaged Navier–Stokes equations. In order to avoid the treatment of complicated boundary conditions on moving walls, the non-inertial reference frame that follows the tank motion is adopted. In this case, the Navier–Stokes equations are modified to be:

$$\frac{\partial \bar{u}_i}{\partial x_i} = 0, \tag{1}$$

$$\frac{\partial \bar{u}_i}{\partial t} + \bar{u}_j \frac{\partial \bar{u}_i}{\partial x_j} = -\frac{1}{\rho}\frac{\partial \bar{p}}{\partial x_i} + \frac{1}{\rho}\frac{\partial}{\partial x_j}\left(\tau_{ij}^m + R_{ij}\right) + f_i, \tag{2}$$

where $i, j = 1, 2, 3$ for 3-D flows, $\bar{u}_i$ denotes the ith component of the filtered (spatially averaged) velocity vector, t the time, ρ the density ($\rho = \rho_a$ in air and $\rho = \rho_w$ in water), $\bar{p}$ the filtered pressure, f_i the ith component of the external acceleration, $\tau_{ij}^m = 2\mu S_{ij}$ the molecular viscous stress tensor with μ being the molecular viscosity, and R_{ij} the stress induced by the filtering process for spatial flow variation that is mainly caused by small-scale turbulence. In the above definition, $S_{ij} = \frac{1}{2}\left(\frac{\partial \bar{u}_i}{\partial x_j} + \frac{\partial \bar{u}_j}{\partial x_i}\right)$ is the rate of strain of the filtered flow. The stress R_{ij} is modeled by the Smagorinsky sub-grid scale (SGS) model from the concept of large-eddy-simulation (LES) [32].

$$R_{ij} = 2\mu_t S_{ij}, \tag{3}$$

where $\mu_t = \rho\left(L_s^2\sqrt{2S_{ij}S_{ij}}\right)$ is the eddy viscosity and L_s is the characteristic length scale which equals $C_s(\Delta x \Delta y \Delta z)^{1/3}$ with $C_s = 0.15$ [24]. For simplicity, the symbol for space filtering, "–", will be dropped from herein.

The external acceleration f_i includes the gravitational acceleration, translational and rotational inertia forces. The vector form of f_i is as follows [18]:

$$\mathbf{f} = \mathbf{g} - \frac{\mathrm{d}\mathbf{V}}{\mathrm{d}t} - \frac{\mathrm{d}\dot{\boldsymbol{\theta}}}{\mathrm{d}t} \times (\mathbf{r} - \mathbf{R}) - 2\dot{\boldsymbol{\theta}} \times \frac{\mathrm{d}(\mathbf{r} - \mathbf{R})}{\mathrm{d}t} - \dot{\boldsymbol{\theta}} \times [\dot{\boldsymbol{\theta}} \times (\mathbf{r} - \mathbf{R})], \tag{4}$$

where $\mathbf{g}$ is the gravitational acceleration; $\mathbf{V}$ and $\dot{\boldsymbol{\theta}}$ are the translational and rotational velocity of the non-inertial frame, respectively; $\mathbf{r}$ and $\mathbf{R}$ are the position vector of the considered point and the rotational motion origin (Fig. 1).

The transportation equation of density is expressed as,

$$\frac{\partial \rho}{\partial t} + u_i \frac{\partial \rho}{\partial x_i} = 0, \tag{5}$$

which implies that the incompressibility of fluid is imposed in the entire two-phase flow field.

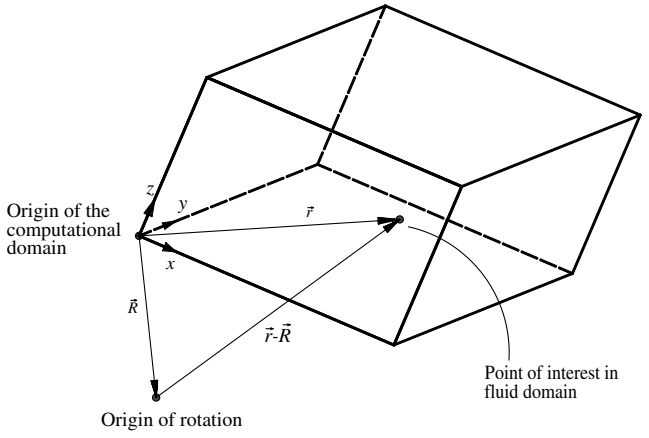

Fig. 1. Non-inertial reference frame for a 3-D tank under external excitation.

3. Numerical implementation

3.1. Two-step projection method and spatial discretization

In the present model, the governing equations are solved by the finite difference method on a staggered grid mesh. A two-step projection method [8,9,22], which has been proved to be very robust, is employed. In the first step, the time derivative is discretized by the forward difference method and an intermediate velocity which carries the correct vorticity is introduced as

$$\frac{\tilde{u}_i^{n+1} - u_i^n}{\Delta t} = -u_j^n \frac{\partial u_i^n}{\partial x_j} + \frac{1}{\rho^n} \frac{\partial \tau_{ij}^n}{\partial x_j}, \tag{6}$$

where the superscript indicates the time level and Δt is the time step size. It is seen that the pressure gradient term and the external acceleration term are not included in Eq. (6), so the intermediate velocity $\tilde{u}_i$ does not, in general, satisfy the continuity equation.

The second step is to project the intermediate velocity field onto a divergence-free plane to obtain the final velocity:

$$\frac{u_i^{n+1} - \tilde{u}_i^{n+1}}{\Delta t} = -\frac{1}{\rho^n} \frac{\partial p^{n+1}}{\partial x_i} + f_i, \tag{7}$$

$$\frac{\partial u_i^{n+1}}{\partial x_i} = 0. \tag{8}$$

Combining (6) and (7), we can show that momentum equations of the SANS equations are satisfied approximately, with pressure gradient being evaluated at the $(n+1)$th time level. Taking the divergence of (7) and applying (8) to the resulting equation yields

$$\frac{\partial}{\partial x_i}\left(\frac{1}{\rho^n} \frac{\partial p^{n+1}}{\partial x_i}\right) = \frac{1}{\Delta t} \frac{\partial \tilde{u}_i^{n+1}}{\partial x_i} + \frac{\partial f_i}{\partial x_i}, \tag{9}$$

which is also called the pressure Poisson equation (PPE). By solving (9) with appropriate boundary conditions iteratively, the correct pressure information at the $(n+1)$th time step will be obtained. Substituting the updated pressure information into (7), the new velocity field at the $(n+1)$th time step, which satisfies the divergence-free constraint enforced by (8), is obtained. As for the spatial discretization, a combination of the central difference method and upwind method is used to discretize the convection terms, while only central difference method is used to discretize the diffusion terms and pressure gradient terms. In addition, the pressure Poisson equation (PPE) is solved by Bi-CGSTAB method [38].

3.2. Interface tracking: VOF method

By introducing a volume-of-fluid function F,

$$F = \frac{\rho - \rho_a}{\rho_w - \rho_a}, \tag{10}$$

Eq. (5) becomes to

$$\frac{\partial F}{\partial t} + u_i \frac{\partial F}{\partial x_i} = 0, \tag{11}$$

where F represents the volumetric ratio between the water (liquid) and the fluid mixture (liquid and gas), which equals to 0 in air and 1 in water, the same as that in the conventional VOF approach.

In the VOF interface tracking method, the normal vector of the interface in each grid is calculated by using Youngs' (least squares) method [31]. The interface will then be moved by the interpolated velocity and the volume flux in all three directions can be calculated according to Gueyffier et al. [15]. After that, the VOF function F can be updated to the next time step. The scheme is second-order accurate. The details of the numerical treatment can be found in Liu [26] and Lin [21].

3.3. Numerical stability criterion

There are two stability criteria that must be satisfied to make the scheme stable. One is related to the convection process that is characterized by the Courant number (Cr) restriction, i.e.

$$\Delta t \leqslant \min\left\{\frac{Cr\times\Delta x}{u_{\max}}, \frac{Cr\times\Delta y}{v_{\max}}, \frac{Cr\times\Delta z}{w_{\max}}\right\}, \tag{12}$$

where $u_{\max}$, $v_{\max}$ and $w_{\max}$ are the maximum velocities in x-, y- and z-direction, respectively. The value of Cr is 1.0 in principle but is often taken below 0.5 to ensure the accuracy and stability in highly non-linear flow regimes.

The other stability restriction is related to the diffusion process. In order to avoid the negative diffusion, the following condition should be satisfied:

$$\Delta t \leqslant \min\left\{\frac{\rho\Delta x^2}{6(\mu+\mu_t)}, \frac{\rho\Delta y^2}{6(\mu+\mu_t)}, \frac{\rho\Delta z^2}{6(\mu+\mu_t)}\right\}. \tag{13}$$

4. Results of 2-D liquid sloshing

In this section, we shall present both the linear and non-linear 2-D sloshing cases. For the former cases, the numerical results will be compared to analytical solution. For the latter cases, the numerical solution will be compared to experimental data and other numerical results.

4.1. Free liquid sloshing for viscous fluids

When the viscous effect is considered, a linearized analytical solution for 2-D small amplitude viscous waves in a rectangular tank has been derived by Wu et al. [36] when the initial interface elevation profile is as follows:

$$\eta_0 = a\cos k\left(x+\frac{W}{2}\right), \tag{14}$$

where W is the length of the tank, a the initial wave amplitude and $k=2\pi/W$. In case when $\kappa=\frac{g}{v^2k^3}>0.5814122$, in which v is the kinematic viscosity of the liquid, the analytical solution for free surface deformation within the basin can be expressed in terms of the following closed-form:

$$\frac{\eta(t)}{\eta_0} = 1-2\kappa Re\sum_{i=1}^{2}\frac{A_i\left\{-\gamma_i e^{(-1+\gamma_i^2)\nu k^2 t}\left[1+\operatorname{erf}(\gamma_i k\sqrt{\nu t})\right]+\gamma_i+\operatorname{erf}(k\sqrt{\nu t})\right\}}{1-\gamma_i^2}, \tag{15}$$

where $Re=h\sqrt{gh}/v$, γ_1 and γ_2 are any two non-conjugate roots of the four possible roots of the equation:

$$(x^2+1)^2-4x+\kappa=0. \tag{16}$$

Writing $\gamma_1=\gamma_{1R}+\mathrm{i}\gamma_{1I}$ and $\gamma_2=\gamma_{2R}+\mathrm{i}\gamma_{2I}$, we have

$$A_1 = -\frac{2}{\Delta}\gamma_{1R}-\mathrm{i}\frac{2\gamma_{1R}^3+1}{\gamma_{1R}\gamma_{1I}\Delta} \quad\text{and}\quad A_2 = -\frac{2}{\Delta}\gamma_{1R}-\mathrm{i}\frac{2\gamma_{1R}^3-1}{\gamma_{1R}\gamma_{2I}\Delta},$$

where $\Delta=4(6\gamma_{1R}^2+1)(2\gamma_{1R}^2+1)-4(\kappa+1)$. It is noted that the origin is set at the left boundary of the tank and on the still water level.

In this simulation, the length of the tank is $W=1$ m. The initial wave amplitude $a=0.01$ m and the still water depth $h=0.5$ m. The turbulence model is turned off in order to compare with the linear analytical solution. The employed mesh system has 25 uniform horizontal grids with the mesh size $\Delta x=0.04$ m and 23 non-uniform vertical grids with 10 grids (the minimum mesh size $\Delta z=0.002$ m) being arranged near the free surface. The constant time step $\Delta t=1.204\times10^{-5}$ s is used in the case of $Re=20$ and $\Delta t=1.204\times10^{-4}$ s in the case of $Re=200$ to provide stable solution during the entire computation. Both cases run up to $t=11.3$ s. It takes about 1.5 and 0.5 CPU hours in Intel (R) Core (TM) 2@1.86 GHz, respectively, to finish

the computation. Fig. 2 shows the numerical results (circle) of the normalized wave elevation $\zeta = \eta/a$ at $x = 0$ against the normalized time $\tau = t\sqrt{g/h}$ when $Re = 20$ and 200. It is seen from the figure that the wave will oscillate with decaying amplitude. The decaying rate of $Re = 20$ is much faster than that of $Re = 200$. In both cases, the numerical results favorably match the analytical solution, indicating the model is a useful tool in predicting the viscous liquid sloshing.

The mesh convergence test is also conducted for both $Re = 20$ and $Re = 200$. The additional computations are made by using the mesh sizes double and half of the previous reference test. The comparisons are plotted in Fig. 2. The difference among three numerical results is small, especially between the reference test and the fine mesh test, implying that the numerical solution is convergent when the reference mesh system is used. The coarse mesh system in the case of $Re = 200$, however, exhibits a faster decaying rate and develops a phase lag after $\tau = 5$.

4.2. Linear forced liquid sloshing under horizontal excitation

In this section, the demonstration will be made by using the present model to simulate liquid sloshing in a horizontally excited 2-D rectangular tank with still water depth h and tank length $2a$. For the periodic excitation, i.e. $u_e = -A\cos\omega t$, where u_e is the tank excitation velocity, $A = b\omega$ is the velocity amplitude with b being the displacement amplitude, and ω is the angular frequency of the excitation, Faltinsen [10] gave the linear analytical solution for the velocity potential function ϕ. One can readily convert ϕ into the free surface displacement η by the use of

$$\eta = \frac{1}{g}\frac{\partial\phi}{\partial t}\bigg|_{z=0}:$$

$$\eta = \frac{1}{g}\sum_{n=0}^{\infty}\sin\left\{\frac{(2n+1)\pi}{2a}x\right\}\cosh\left\{\frac{(2n+1)\pi}{2a}h\right\}[-A_n\omega_n\sin\omega_n t - C_n\omega\sin\omega t] - \frac{1}{g}A\omega x\sin\omega t, \tag{17}$$

where

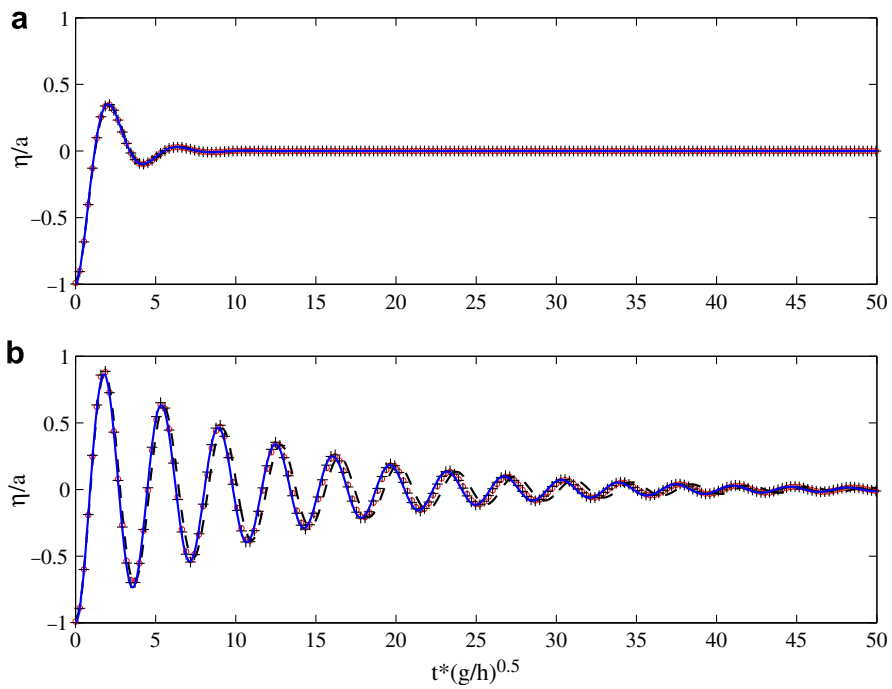

Fig. 2. Comparison of the time series τ of normalized free surface elevation at $x = 0$ between the present numerical results using reference mesh (25×23: circle), fine mesh (50×43: plus sign), coarse mesh (13×14: dashed line) and analytical solution (solid line) when (a) $Re = 20$; (b) $Re = 200$.

$$\omega_n^2 = g\frac{(2n+1)\pi}{2a}\tanh\left\{\frac{(2n+1)\pi}{2a}h\right\}, \quad C_n = \frac{\omega K_n}{\omega_n^2-\omega^2}, \quad A_n = -C_n - \frac{K_n}{\omega},$$
$$K_n = \frac{\omega A}{\cosh\left\{\frac{(2n+1)\pi}{2a}h\right\}}\frac{2}{a}\left[\frac{2a}{(2n+1)\pi}\right]^2(-1)^n. \tag{18}$$

It is noted that the origin is set at the center of the tank and on the still water level.

In this study, we will use the parameter $h = a = 0.5$ m. With $g = 9.81$ m/s^2, the lowest natural frequency of fluid in the tank can be computed as $\omega_0 = 5.314$ s^{-1}. We first simulate the case with the excitation frequency $\omega = 0.5\omega_0$ and $b = 0.01$ m. The turbulence model is turned off and the molecular viscosity is set to zero to be consistent with potential flow assumption. In the simulation, the employed mesh system has 100 uniform horizontal meshes with mesh size $\Delta x = 0.01$ m and 50 non-uniform vertical meshes with 27 grids (the minimum $\Delta z = 0.001$ m) being arranged near the free surface. The time step is automatically adjusted to ensure the numerical stability. The simulation runs up to $t = 10$ s. It takes about 0.4 CPU hours in Intel (R) Core (TM) 2@1.86 GHz to finish the computation. The numerical results of free surface displacement at $x = a$ (right boundary) are compared to the analytical solution (17) in Fig. 3a. Very good agreements are obtained in the comparison.

The model is then used to study the liquid sloshing at the near-resonant frequency of $\omega = 0.95\omega_0$. This time the displacement amplitude is set to be very small, i.e. $b = 0.0004$ m. In this simulation, the employed mesh system has 100 uniform horizontal meshes with mesh size $\Delta x = 0.01$ m and 43 non-uniform vertical meshes with 20 grids (the minimum $\Delta z = 0.001$ m) being arranged near the free surface. It used 0.3 CPU hours in this computation. Although the displacement amplitude is only 4% of that in the first case, due to the resonance effect, the sloshing amplitude grows to the same order of magnitude at $t = 10$ s, as shown in Fig. 3b. Again, the numerical results match remarkably well with the theory. The numerical experiments presented in this section demonstrate the model's accuracy in terms of free surface displacement calculation under external excitation.

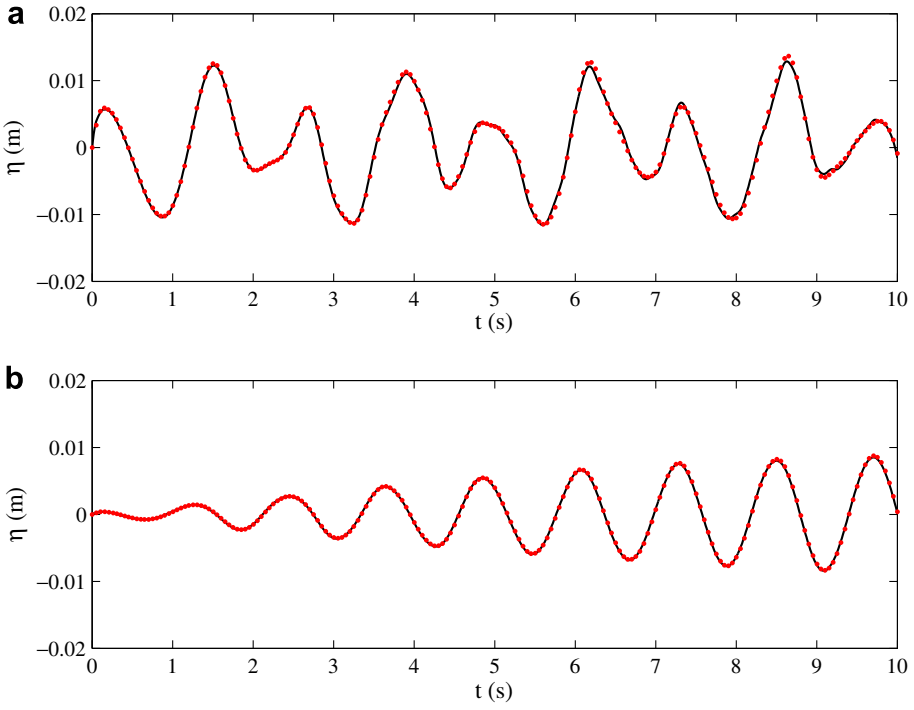

Fig. 3. Comparisons of free surface displacement at $x = a$ in a horizontally excited tank with (a) $b = 0.01$ m and $\omega = 0.5\omega_0$; (b) $b = 0.0004$ m and $\omega = 0.95\omega_0$ between the present numerical results (dotted line) and analytical solution (solid line).

4.3. Non-linear liquid sloshing under surge motion

The previous comparisons are within linear regime, i.e. $H/h \ll 1$. In order to test the performance of the present model in solving non-linear wave, two experiments are conducted for both non-resonance and resonance cases.

The experiments have been conducted in a hexahedron tank which is 570 mm long, 310 mm wide, and 300 mm high in the Structural Laboratory at National University of Singapore. The water depth is 150 mm, so the lowest natural frequency $\omega_0 = 6.0578\ \mathrm{s}^{-1}$. The tank is secured on a shaker. Two experiments with different shaking frequencies but the same amplitude are conducted. The movement of the shaker follows the sinusoidal function:

$$x = -a \sin \omega t,$$

where the amplitude $a = 5$ mm and the shaking frequencies ω are $0.583\omega_0$ and $1.0\omega_0$, respectively. The wave tank is equipped with three wave gauges which are located at the center of the tank, near the left boundary and the right boundary of the tank (Fig. 4).

In this first simulation, the employed mesh system has 114 uniform horizontal meshes with mesh size $\Delta x = 0.005$ m and 43 non-uniform vertical meshes with 20 grids (the minimum $\Delta z = 0.005$ m) being arranged near the free surface. The time step is automatically adjusted to ensure the numerical stability. The simulation with $\omega = 0.583\omega_0$ runs up to $t = 22.5$ s. The turbulence model is turned on in this case to simulate the real fluid. It used 0.5 CPU hours in this computation. The numerical results of free surface displacement at the positions of the probes (Fig. 4) are compared to the experimental data and analytical solution. Very good agreements are obtained in all three positions (Fig. 5) among the numerical, analytical and experiment results. In this case, another simulation with the turbulence model being turned off is also performed. Bare difference can be observed between the two simulations, implying that turbulence effect is negligible in this case.

In the second simulation where $\omega = 1.0\omega_0$, the employed mesh system has 114 uniform horizontal meshes with mesh size $\Delta x = 0.005$ m and 64 uniform vertical meshes with $\Delta z = 0.005$ m. The simulation with $\omega = 1.0\omega_0$ runs up to $t = 6.7$ s. It took 0.9 CPU hours to finish this case. Very obvious resonant phenomenon is shown in Fig. 6. In addition, the linear analytical solution, which shows symmetric wave pattern, fails because the wave crest is much larger than the trough in this resonant case. Therefore, we will compare the wave amplitude with the experiment data. From Fig. 6, it can be seen that the present numerical results agree

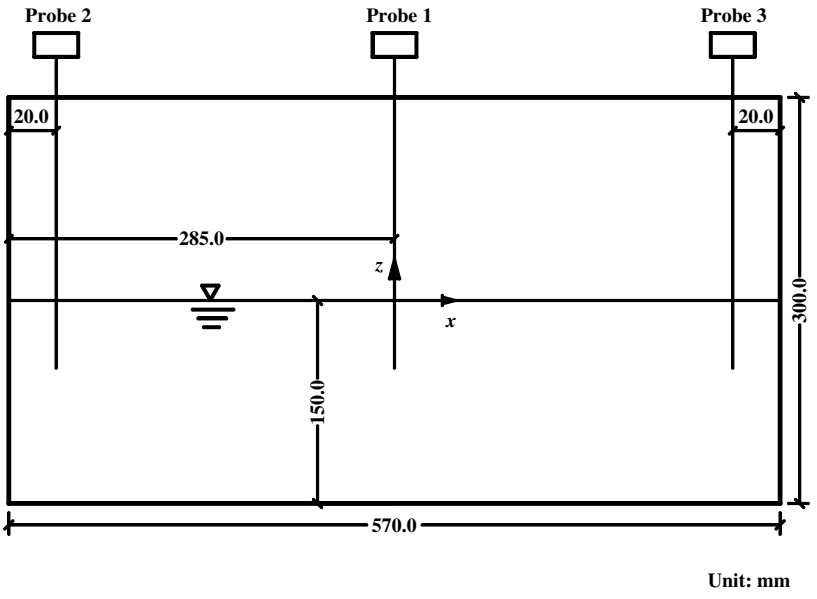

Fig. 4. The sketch of the 2-D sloshing experiment.

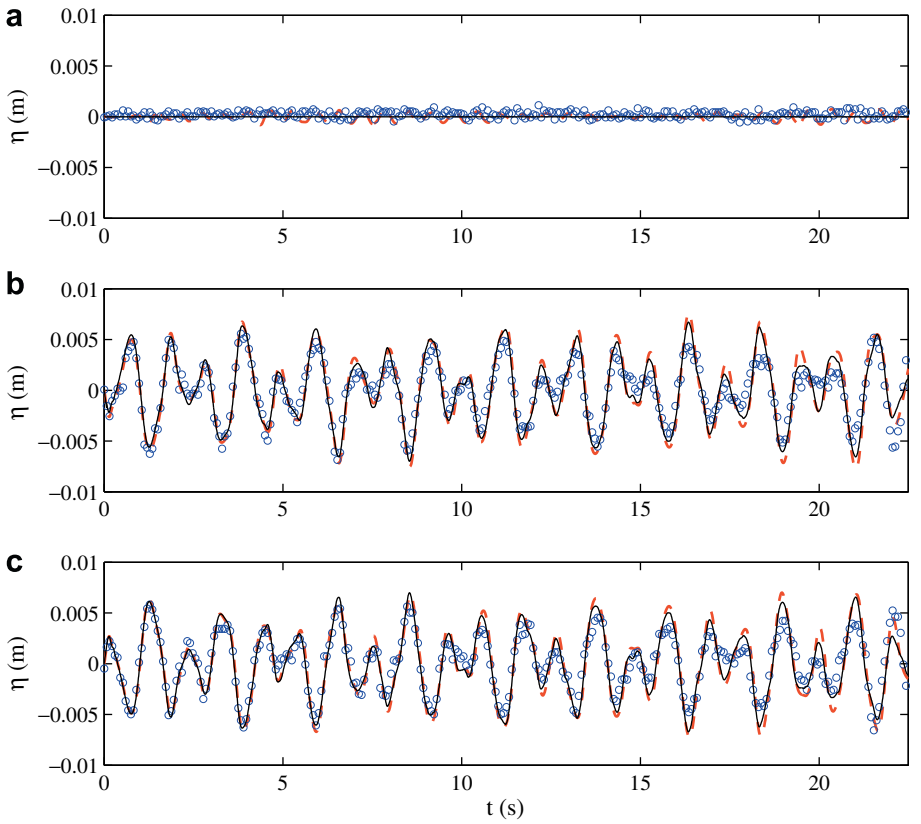

Fig. 5. Comparisons of the time series of surface elevation η at the position of (a) probe 1; (b) probe 2; and (c) probe 3 among the present numerical results (dashed line), the analytical solution (solid line) and experimental data (circle) when $\omega = 0.583\omega_0$.

very well both experiment data and the solution of another NSE solver with σ-coordinate transformation [23], indicating that the present model is an accurate tool in predicting the non-linear sloshing motion. Whether the turbulence model is on or off makes little difference to the final results in this case.

5. Results of 3-D liquid sloshing

5.1. Free sloshing

In the following paragraphs, the 3-D liquid sloshing in a confined tank will be studied and discussed. The tank has the dimensions of $L_x \times L_y$. For the initial free surface displacement being Gaussian distribution about the center of the basin, i.e.

$$\eta_0(x,y) = H_0 \exp\left\{-\beta[(x - L_x/2)^2 + (y - L_y/2)^2]\right\}, \tag{19}$$

where H_0 is the initial height of the hump and β is the peak enhancement factor, Wei and Kirby [34] proposed the linear analytical solution for the free surface deformation within the basin:

$$\eta(x,y,t) = \sum_{n=0}^{\infty}\sum_{m=0}^{\infty} \bar{\eta}_{nm} e^{-i\omega_{nm}t} \cos(n\lambda x)\cos(m\lambda y) \tag{20}$$

in which:

$$\bar{\eta}_{nm} = \frac{4}{(1+\delta_{n0})(1+\delta_{m0})L_xL_y}\int_0^{L_x}\int_0^{L_y} \eta_0(x,y)\cos(n\lambda x)\cos(m\lambda y)\mathrm{d}x\,\mathrm{d}y, \tag{21}$$

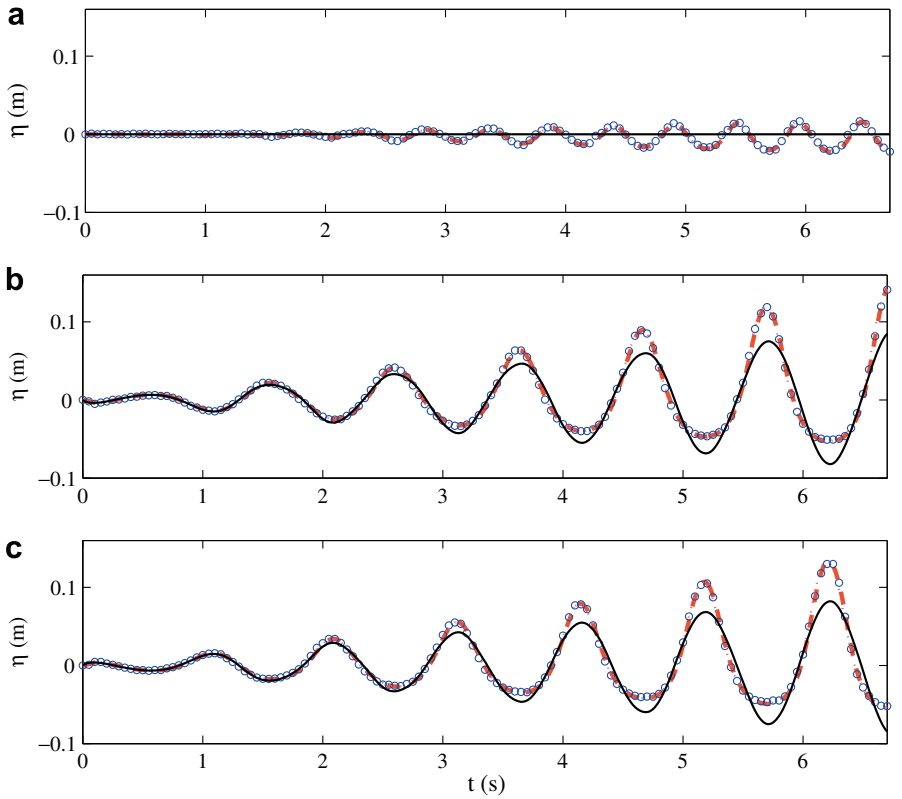

Fig. 6. Comparisons of the time series of surface elevation η at the position of (a) probe 1; (b) probe 2; and (c) probe 3 among the present numerical results (dashed line), the analytical solution (solid line), the numerical results of σ-coordinate model [23] (dotted line) and experimental data (circle) when $\omega = 1.0\omega_0$.

where δ_{nm} is the Kronecker delta function and

$$\lambda = \frac{\pi}{L_x} = \frac{\pi}{L_y}. \tag{22}$$

The (n,m) wave modes have the corresponding natural frequency that is determined by the linear dispersion equation,

$$\omega_{nm}^2 = g k_{nm} \tanh(k_{nm} h_0), \tag{23}$$

where h_0 is the still water depth and

$$k_{nm}^2 = (n\lambda)^2 + (m\lambda)^2 = \left(\frac{\pi}{L_x}\right)^2 (n^2 + m^2). \tag{24}$$

In this study, we take the following parameters: $L_x = L_y = 10$ m, $h_0 = 0.50$ m, $H_0 = 0.05$ m, and $\beta = 0.4$. The ratio of the initial height of the hump to the water depth $H_0/h_0 = 0.1$, which is relatively small, so only a little non-linearity is present during the wave transformation and we can use this case to validate the accuracy and stability of this model. The domain is discretized by 200×200 uniform grids with $\Delta x = \Delta y = 0.05$ m in the horizontal plane and 21 non-uniform grids with eight grids (the minimum $\Delta z = 0.01$ m) near the interface are used in the vertical direction. The time step is adjusted automatically to ensure the stability of the model. The turbulence model is again turned off. The simulation runs up to $t = 50$ s and it took abound 20 CPU hours to finish this case.

The comparisons of the time histories of surface elevation at the center of the domain among the present numerical results, the analytical solutions, the Boussinesq solutions [25] and another NSE solver using

σ-coordinate transformation [23] are shown in Fig. 7a. It is found that the Boussinesq solutions have a little larger phase shift from the analytical solution than the other two numerical results, although the wave pattern is almost the same as the analytical solution. On the other hand, both of the other two NSE results favorably match the analytical solution, indicating the present model is good enough in predicting the wave amplitude when the H_0/h_0 ratio is small.

If the initial height of the hump H_0 is increased to 0.20 m, the strong wave non-linearity is present and the linear wave theory fails to describe the wave pattern from the very first wave (Fig. 7b). The Boussinesq results agree fairly well with both NSE solutions in the beginning, but discrepancies develop later mainly for the phase calculations. This implies that as the wave non-linearity becomes very strong, the accuracy of the Boussinesq equations can be degenerated. However, the results of present model compared very well with the other NSE solver using σ-coordinate transformation, indicating the present numerical model can accurately simulate the wave problem with strong non-linearity.

5.2. Linear forced sloshing under combined surge and sway excitations

In this section, the validation will be further made by using the present model to simulate liquid sloshing in a 3-D hexahedron tank with still water depth h, tank length $2a$ and width $2w$. If the tank was set on a shaking table making an angle φ from the axis of oscillation, for a periodic excitation of the shaker, i.e. $u_e = -A\cos\omega t$, where u_e is the shaker excitation velocity, $A = b\omega$ is the velocity amplitude with b being the displacement amplitude, and ω is the angular frequency of the excitation, we can project the velocity of the shaker u_e into x- and y-direction (Fig. 8) and consider the problem to be a coupled surge and sway motion, i.e.

$$u_x = -A\cos\varphi\cos\omega t,$$
$$u_y = -A\sin\varphi\cos\omega t.$$

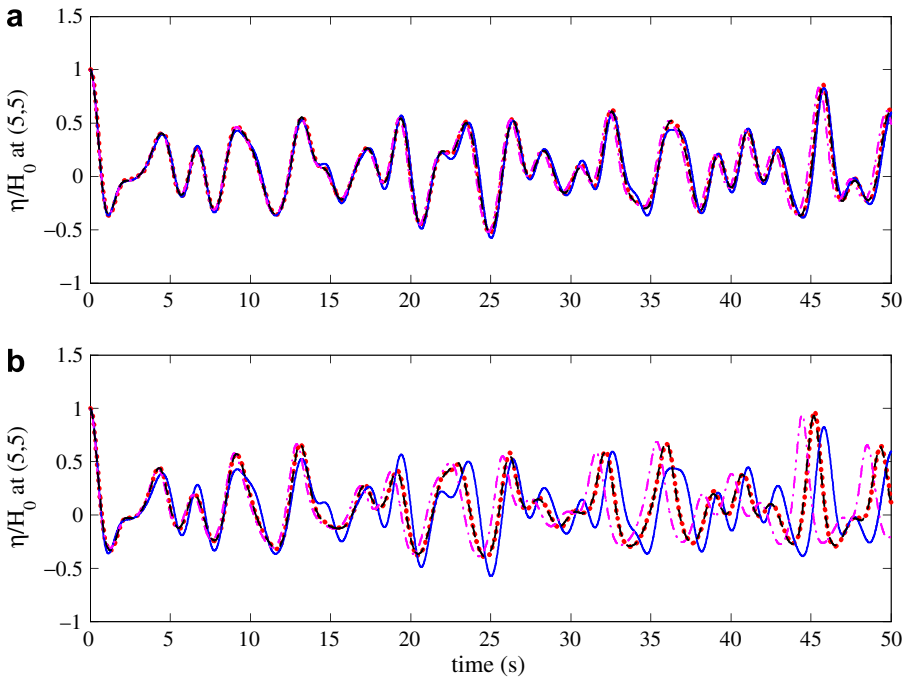

Fig. 7. Comparisons of the time series of normalized surface elevation η/H_0 at the center of the tank among the present numerical results (dotted line), another NSE solver [23] (dashed line), the Boussinesq equation solver [25] (dash-dot line) and linear analytical solution (solid line) for (a) $H_0/h_0 = 0.1$; (b) $H_0/h_0 = 0.4$.

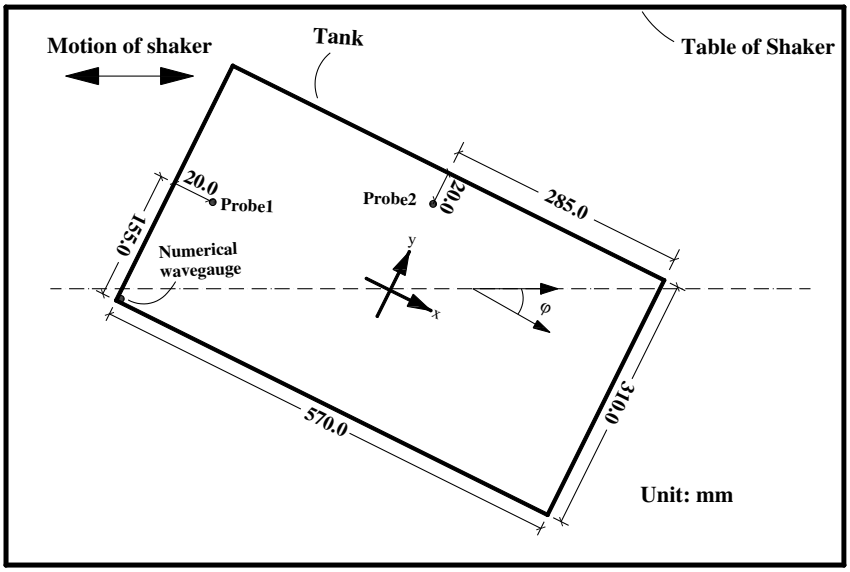

Fig. 8. Top view of the 3-D experiment set of the tank on the shaker table.

Combining the linear analytical solution of Faltinsen [10] under 1-D excitation, which has been discussed in Section 4.2, in both x-direction and y-direction, the 3-D linear analytical solution of surface elevation of combined surge and sway excitations is as follows:

$$\eta = \frac{1}{g}\sum_{n=0}^{\infty} \sin\left\{\frac{(2n+1)\pi}{2a}x\right\} \cosh\left\{\frac{(2n+1)\pi}{2a}h\right\}[-A_{nx}\omega_{nx}\sin\omega_{nx}t - C_{nx}\omega\sin\omega t] - \frac{1}{g}A\omega x\sin\omega t + \frac{1}{g}\sum_{n=0}^{\infty} \sin\left\{\frac{(2n+1)\pi}{2w}y\right\} \cosh\left\{\frac{(2n+1)\pi}{2w}h\right\}[-A_{ny}\omega_{ny}\sin\omega_{ny}t - C_{ny}\omega\sin\omega t] - \frac{1}{g}A\omega y\sin\omega t, \quad (25)$$

where

$$\omega_{nx}^2 = g\frac{(2n+1)\pi}{2a}\tanh\left\{\frac{(2n+1)\pi}{2a}h\right\}, \quad C_{nx} = \frac{\omega K_{nx}}{\omega_{nx}^2-\omega^2} \quad A_{nx} = -C_{nx} - \frac{K_{nx}}{\omega},$$
$$K_{nx} = \frac{\omega A}{\cosh\left\{\frac{(2n+1)\pi}{2a}h\right\}}\frac{2}{a}\left[\frac{2a}{(2n+1)\pi}\right]^2(-1)^n \quad (26)$$

and

$$\omega_{ny}^2 = g\frac{(2n+1)\pi}{2w}\tanh\left\{\frac{(2n+1)\pi}{2w}h\right\}, \quad C_{ny} = \frac{\omega K_{ny}}{\omega_{ny}^2-\omega^2} \quad A_{ny} = -C_{ny} - \frac{K_{ny}}{\omega},$$
$$K_{ny} = \frac{\omega A}{\cosh\left\{\frac{(2n+1)\pi}{2w}h\right\}}\frac{2}{w}\left[\frac{2w}{(2n+1)\pi}\right]^2(-1)^n. \quad (27)$$

It is noted that the origin is still set at the center of the tank and on the still water level.

In this section, we will use the parameter $h = 0.15$ m, $a = 0.285$ m and $w = 0.155$ m. The natural frequencies in this case are [35]:

$$\omega_{mn}^2 = \sqrt{\left(\frac{mg\pi}{2a}\right)^2 + \left(\frac{ng\pi}{2w}\right)^2}\tanh\sqrt{\left(\frac{m\pi h}{2a}\right)^2 + \left(\frac{n\pi h}{2w}\right)^2} \quad (m,n = 0,1,2,\ldots). \quad (28)$$

The lowest natural frequencies are $\omega_{10} = 6.0578\ s^{-1}$ and $\omega_{01} = 9.5048\ s^{-1}$, respectively. We will first simulate the case with the excitation frequency $\omega = 3.635\ s^{-1}$, which is away from the natural frequency of the tank, and $b = 0.005$ m. The tank is set on a shaking table making an angle $\varphi = 30°$ from the axis of oscillation. In the entire sloshing process, the sloshing amplitude will remain small and the linear theory in (25) applies.

In the numerical simulation, the domain is discretized by 114×62 uniform grids with $\Delta x = \Delta y = 0.005$ m in the horizontal plane and 45 non-uniform grids with 25 grids (the minimum $\Delta z = 0.001$ m) near the free surface are used in the vertical direction. The time step is automatically adjusted to ensure the numerical stability. The simulation runs up to $t = 20$ s and it took about 55 CPU hours to finish this case. The snap shots of the free surface at $t = 0.0$, 4.0, 8.0, 12.0, 16.0 and 20.0 s are shown in Fig. 9, where we can see the obvious 3-D free surface. The numerical results of free surface displacement at the center and corner of the tank are compared to the analytical solution (25) in Fig. 10. Very good agreements are obtained in the comparison. The numerical

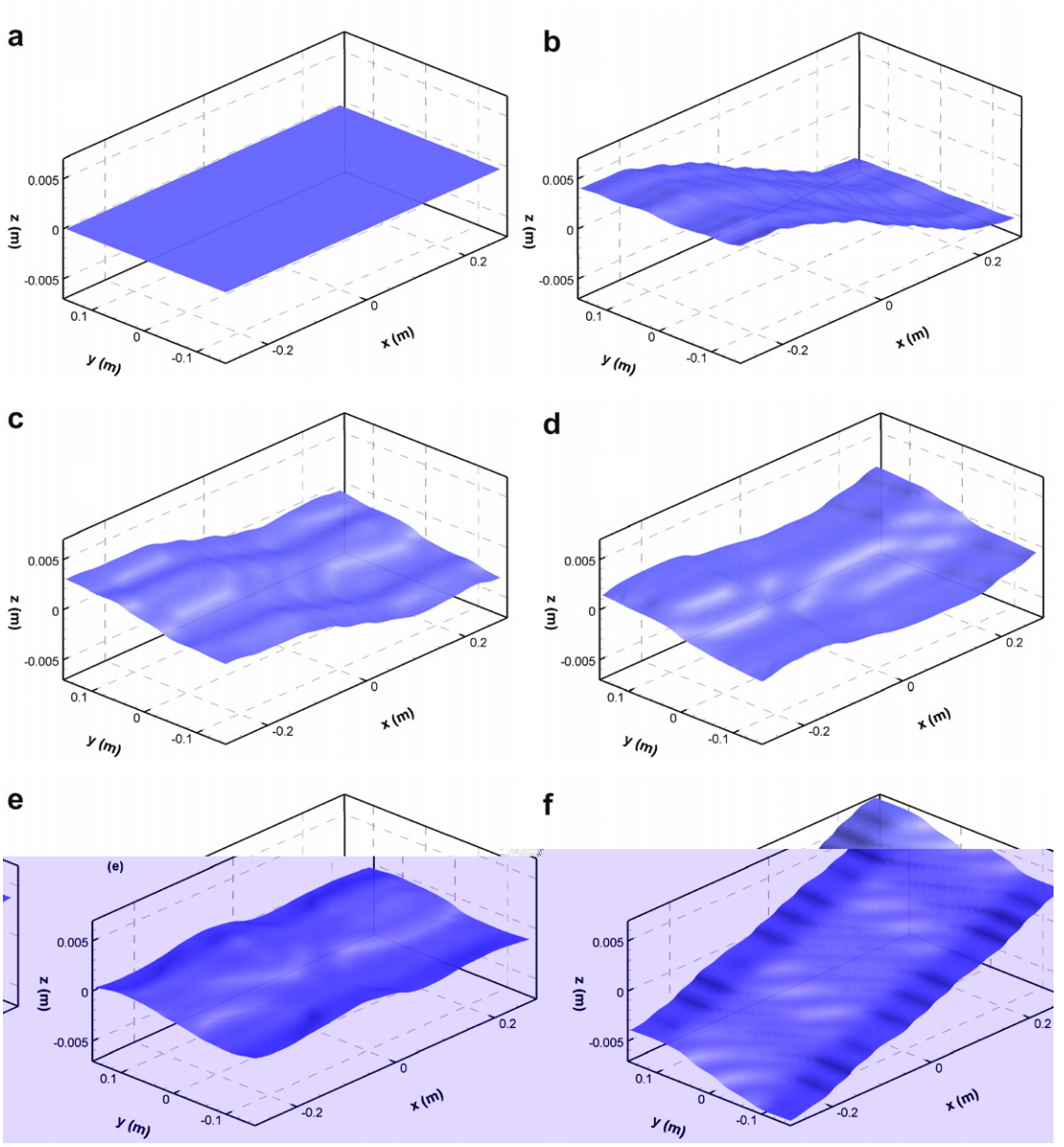

Fig. 9. Snap shots of free surface profiles during 3-D forced sloshing at $t = 0.0$, 4.0, 8.0, 12.0, 16.0 and 20.0 s.

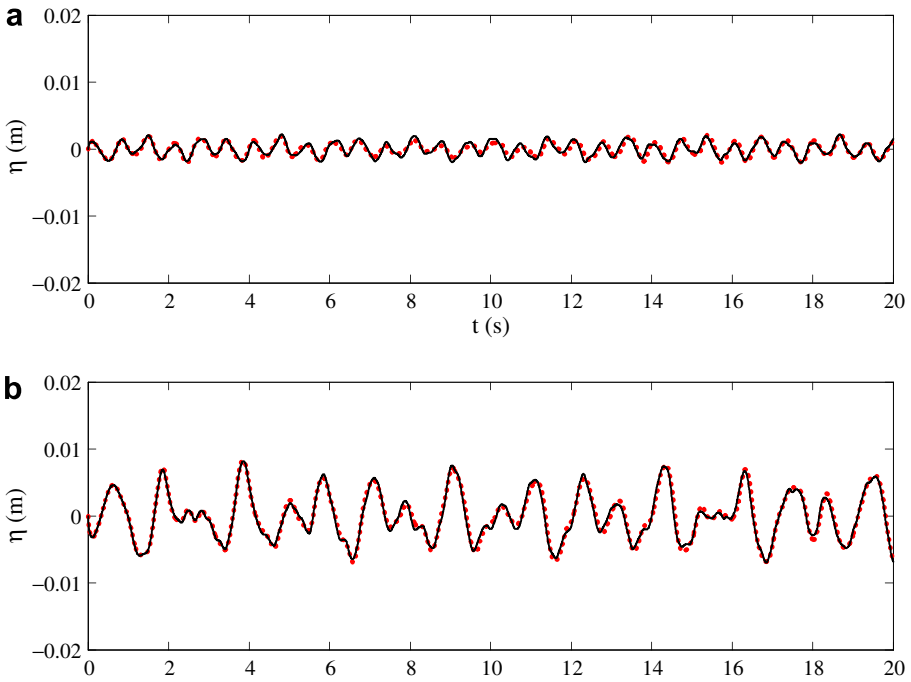

Fig. 10. Comparisons of the time series of surface elevation η at (a) (0.0, 0.155) and (b) the corner (−0.285, −0.155) of the tank between the present numerical results (dotted line), and linear analytical solution (solid line).

experiment presented in this section demonstrates the model's accuracy in terms of coupled surge and sway sloshing motion.

5.3. Nonlinear forced sloshing near resonance

In order to investigate the non-linearity and resonance phenomenon of sloshing under the coupled surge and sway sloshing motion, a series of numerical test is conducted in the tank with the same dimension used in Section 5.2. However, we will choose $\omega = 0.985\omega_{10}$ so that the near resonance phenomenon will occur. In this first simulation, the amplitude of excitation is purposely kept to be very small ($b = 0.0005$ m) so that the problem remains linear in the entire simulation. In the second simulation, the larger amplitude of excitation $b = 0.005$ m, which is the actual value used in the laboratory experiment, is adopted. In the former case, the domain is discretized by a mesh system that has a uniform horizontal mesh size $\Delta x = \Delta y = 0.005$ m and 34 non-uniform vertical meshes with 14 grids (the minimum $\Delta z = 0.002$ m) being arranged near the free surface. In the latter case, the domain is discretized by $114 \times 62 \times 30$ uniform grids with $\Delta x = \Delta y = 0.005$ m and $\Delta z = 0.01$ m. The time step is automatically adjusted to ensure numerical stability. Both simulations run up to $t = 8$ s. It used 18 CPU hours in the former case and 52 CPU hours in the latter case. For the latter case, strong non-linearity will present in the sloshing. Two wave probes are used to measure the free surface displacement and they are located at (−0.265, 0.0) m for Probe 1 and (0.0, 0.135) m for Probe 2 (Fig. 8). One more numerical wave gauge is placed at the corner of the tank (−0.285, −0.155) m.

The normalized free surface elevations at three positions are compared with the analytical solution for the small excitation and experimental data for the large excitation (Fig. 11). It is shown that both cases generate resonance phenomenon. When the excitation amplitude is small, the numerical results agree very well with the linear analytical solution at all positions. However, as the excitation amplitude increases, the free surface elevation deviates significantly from the linear solution; instead it matches well with the experimental data. Furthermore, the wave crest becomes sharper and the trough becomes flatter, a typical phenomenon in non-linear wave. All of these demonstrate the good performance of the model in simulating 3-D strongly non-linear liquid sloshing.

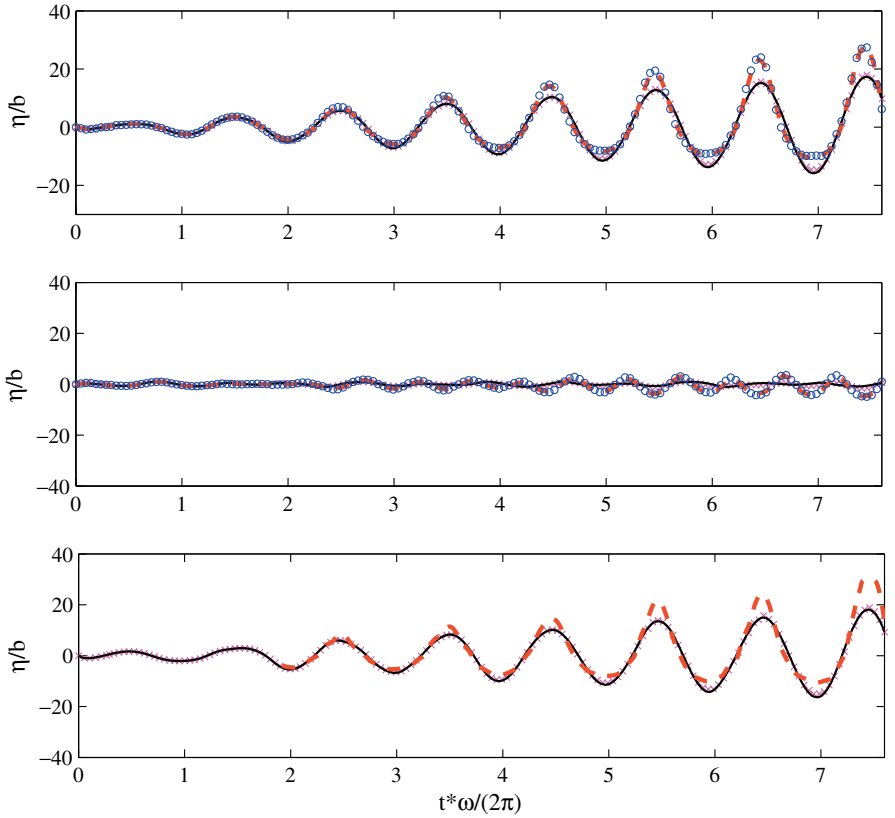

5.4. Violent forced sloshing with broken free-surface

In this section, the study of 3-D liquid sloshing in a confined tank with six DOF of motion is investigated. The horizontal tank dimension is the same as that in Sections 5.2 and 5.3 while the height of the tank is set to 0.3 m. The initial still water depth $h = 0.24$ m so that 80% of the tank is filled with water. The excitation frequencies of all six DOF are set to be $\omega = 3.635\ \mathrm{s}^{-1}$, which is away from the natural frequency of the water in the tank.

The translating motions of excitation are:

Surge: $u_e = b_1\omega\cos\varphi\cos(\omega t)$;
Sway: $v_e = b_2\omega\sin\varphi\cos(\omega t)$;
Heave: $w_e = b_3\omega\cos(\omega t)$;

where $b_1 = b_2 = 0.08$ m, $b_3 = 0.02$ m, and $\varphi = 30°$.

The rotating motions of excitation are:

Pitch: $\dot{\theta}_{1e} = \theta_1\omega\cos(\omega t)$;
Roll: $\dot{\theta}_{2e} = \theta_2\omega\cos(\omega t)$;
Yaw: $\dot{\theta}_{3e} = \theta_3\omega\cos(\omega t)$;

where $\theta_1 = 10°$, $\theta_2 = 10°$ and $\theta_3 = 2°$.

The domain is discretized by $57 \times 31 \times 30$ uniform grids with $\Delta x = \Delta y = \Delta z = 0.01$ m. The time step is automatically adjusted to ensure numerical stability. The simulation runs up to $t = 50$ s. It takes about 265 CPU hours to complete this case in IBM XSERIES_3650 Intel (R) Xeon(R) CPU X5355@2.66 GHz.

The simulation results of the sloshing water are shown in Fig. 12. As most of the tank space is filled with water and the excitation amplitude is large, the sloshing water will hit the ceiling of the tank. The plunging wave is formed that generates many water droplets when the free surface is broken.

The time histories of the free surface elevation, which is estimated by integrating the VOF function in vertical direction, at (0.0, 0.0), (−0.15, −0.08) and (−0.285, −0.155) m are shown in the left column of Fig. 13. It can be seen that the wave amplitude at the corner is much larger than that at the center. Due to the ceiling effect, the growth of positive free surface displacement is restricted as shown in Fig. 13c. Using the fast Fourier transform (FFT) technique, we can obtain the corresponding wave energy density spectrum (right column of Fig. 13). The dominant frequency of the energy density is 0.58 Hz, which is equal to the frequency of the external excitation. The second peak corresponds to 1.16 Hz, a little larger than the lowest theoretical natural frequency 0.96 Hz. This probably arises from the ceiling effect that increases the effective sloshing frequency. The turbulence energy resolved by the LES is comparably small and decays as the increase of frequency. The above simulation demonstrates the capability of the model in simulating violent liquid sloshing with broken free surfaces.

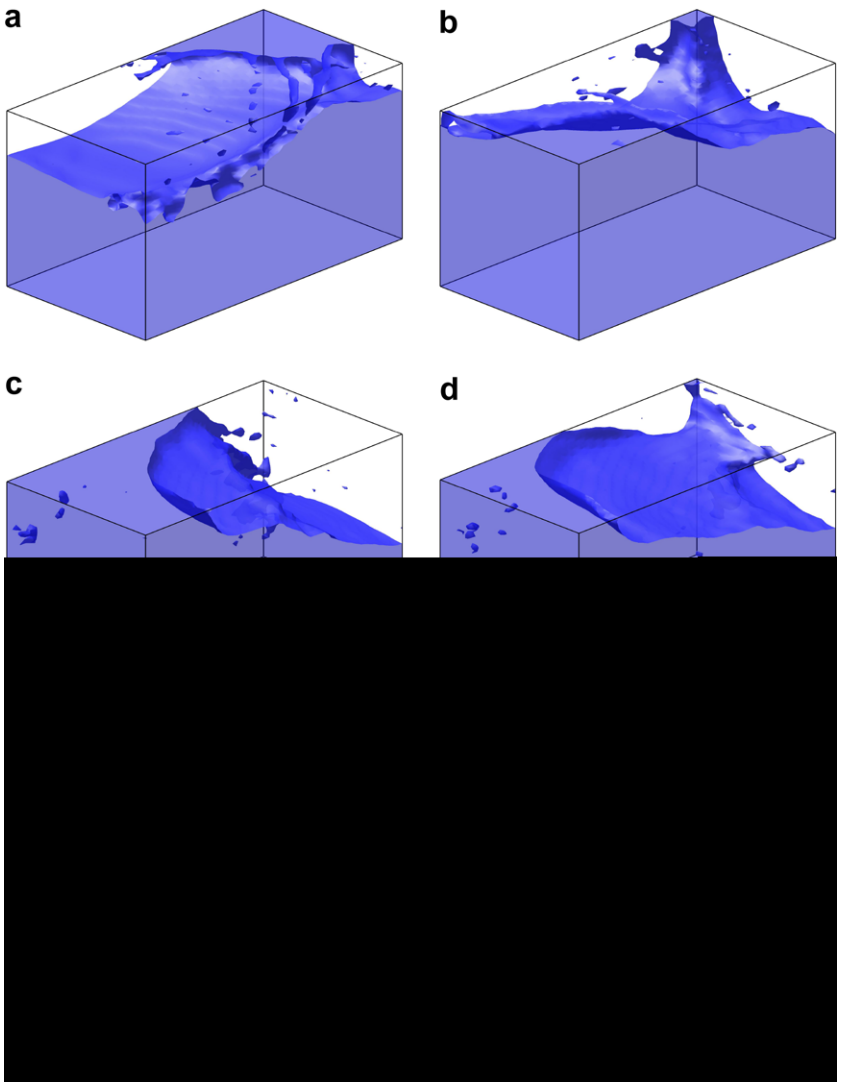

Fig. 12. Snap shots of violent sloshing at $t = 0.4$, 0.6, 0.9, 1.0, 1.2 and 1.6 s.

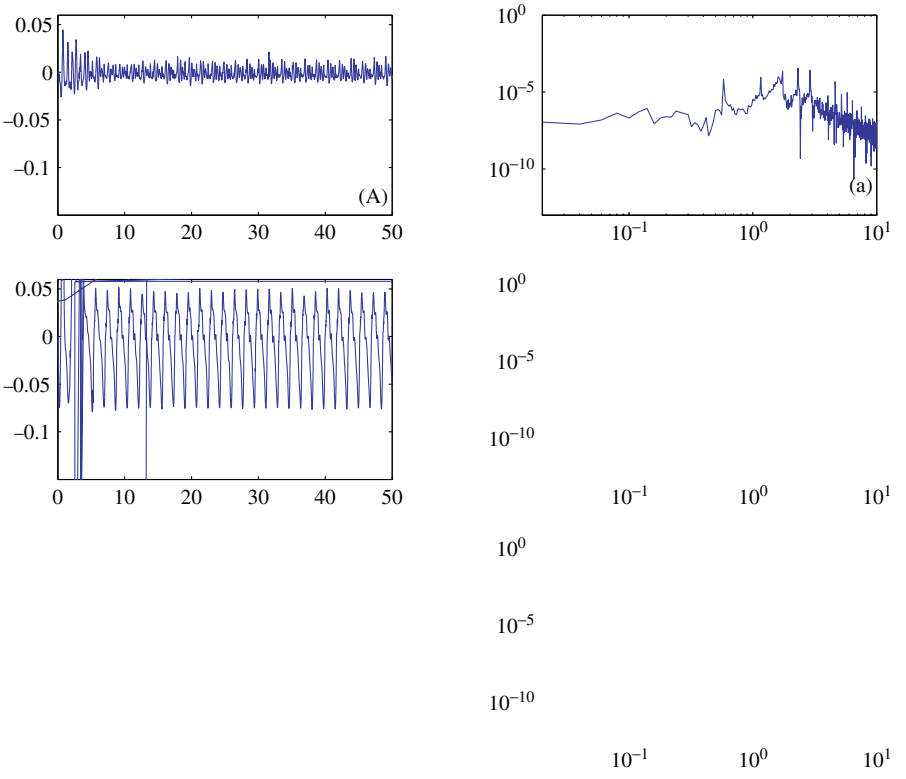

6. Conclusion

In this study, a 3-D two-phase fluid flow model NEWTANK is developed to solve the spatially averaged Navier–Stokes equations. The model is employed to study 2-D and 3-D viscous and inviscid liquid sloshing in rectangular tanks. The model has the capability of simulating highly non-linear and turbulent sloshing processes with broken free surfaces under arbitrarily six DOF external excitations. Laboratory experiments are conducted for both 2-D and 3-D water sloshing under the external excitation of surge and sway motion, in order to provide the experimental data for model validation. Furthermore, a linear analytical solution for 3-D sloshing is proposed to provide the basis of model verification.

The model is first validated against available theories and experimental data for 2-D sloshing of both viscous and inviscid fluids. For small amplitude sloshing, the numerical results agree excellently with all of the linear theories. For large amplitude sloshing, the numerical results deviate significantly from the linear analytical solution. Instead, they match well with the experimental data that exhibit obvious non-linear wave effects.

The model validation is further extended to 3-D liquid sloshing and the comparisons are made to available linear theories, experimental data, and numerical results from other numerical models (e.g. Boussinesq model and Navier–Stokes equation model constructed on σ-coordinate). Again, the numerical results compare very well with the available linear theories when the sloshing amplitude is small. As the increase of the sloshing amplitude, large discrepancies between the numerical results and the analytical solutions are developed because of the strong wave non-linearity present in the sloshing process. Under this circumstance, the present numerical results agree well with the available experimental data and the numerical results calculated by the σ-coordinate model.

Finally as the demonstration, the violent liquid sloshing under six DOF excitations is simulated. The sloshing contains broken free-surface and strong turbulence. The study present in this paper shows that the present model is a promising numerical tool for simulating highly non-linear liquid sloshing in a rigid tank. Future study, however, is still required to quantify the turbulence effect on energy dissipation and the strong impulsive pressure generated by broken free surface during sloshing process. The effect of baffles on sloshing is also being studied, which shall be reported later separately.

Acknowledgments

The authors wish to thank Prof. Koh Chan Ghee and Ms. Gao Mimi in National University of Singapore for providing the experimental data of 2-D and 3-D sloshing. The research was supported, in part, by research grants from Natural Science Foundation of China (NSFC Nos.: 50525926 and 50679046), National Science & Technology Plan 973 (2007CB714105), and the National University of Singapore (R-264-000-182-112).

References

[1] H. Akyildiz, E. Ünal, Experimental investigation of pressure distribution on a rectangular tank due to the liquid sloshing, Ocean Eng. 32 (2005) 1503–1516.
[2] V. Armenio, M. La Rocca, On the analysis of sloshing of water in rectangular containers: numerical and experimental investigation, Ocean Eng. 23 (1996) 705–739.
[3] W. Chen, M.A. Haroun, F. Liu, Large amplitude liquid sloshing in seismically excited tanks, Earthquake Eng. Struct. Dyn. 25 (1996) 653–669.
[4] B.-F. Chen, H.-W. Chiang, Complete 2D and fully nonlinear analysis of ideal fluid in tanks, J. Eng. Mech.-ASCE 125 (1999) 70–78.
[5] B.-F. Chen, Viscous fluid in a tank under coupled surge, heave and pitch motions, J. Waterw. Port Coast. Ocean Eng.-ASCE 131 (2005) 239–256.
[6] B.-F. Chen, R. Nokes, Time-independent finite difference analysis of 2D and nonlinear viscous liquid sloshing in a rectangular tank, J. Comput. Phys. 209 (2005) 47–81.
[7] J.R. Cho, H.W. Lee, Non-linear finite element analysis of large amplitude sloshing flow in two-dimensional tank, Int. J. Numer. Method Eng. 61 (2004) 514–531.
[8] A.J. Chorin, Numerical solution of the Navier–Stokes equations, Math. Comput. 22 (1968) 745–762.
[9] A.J. Chorin, On the convergence of discrete approximations of the Navier–Stokes equations, Math. Comput. 232 (1969) 341–353.
[10] O.M. Faltinsen, A numerical nonlinear method of sloshing in tanks with two-dimensional flow, J. Ship Res. 22 (1978) 193–202.
[11] O.M. Faltinsen, O.F. Rognebakke, I.A. Lukovsky, A.N. Timokha, Multidimensional modal analysis of nonlinear sloshing in a rectangular tank with finite water depth, J. Fluid Mech. 407 (2000) 201–234.
[12] O.M. Faltinsen, A.N. Timokha, Adaptive multimodal approach to nonlinear sloshing in a rectangular tank, J. Fluid Mech. 432 (2001) 167–200.
[13] J.B. Frandsen, A.G.L. Borthwick, Simulation of sloshing motions in fixed and vertically excited containers using a 2-D inviscid σ-transformed finite difference solver, J. Fluid Struct. 18 (2003) 197–214.
[14] J.B. Frandsen, Sloshing motions in excited tanks, J. Comput. Phys. 196 (2004) 53–87.
[15] D. Gueyffier, J. Li, A. Nadim, R. Scardovelli, S. Zaleski, Volume-of-fluid interface tracking with smoothed surface stress methods for 3-D flows, J. Comput. Phys. 152 (1999) 423–456.
[16] D.F. Hill, Transient and steady-state amplitudes of forced waves in rectangular basins, Phys. Fluid 15 (2003) 1576–1587.
[17] R.A. Ibrahim, V.N. Pilipchuk, T. Ikeda, Recent advances in liquid sloshing dynamics, Appl. Mech. Rev. 54 (2001) 133–199.
[18] R.A. Ibrahim, Liquid Sloshing Dynamics: Theory and Applications, Cambridge University Press, New York, USA, 2005.
[19] Y. Kim, Numerical simulation of sloshing flows with impact load, Appl. Ocean Res. 23 (2001) 53–62.
[20] Y. Kim, Y.-S. Shin, K.H. Lee, Numerical study on slosh-induced impact pressures on 3-D prismatic tanks, Appl. Ocean Res. 26 (2004) 213–226.
[21] P. Lin, Numerical Modeling of Water Waves, Taylor & Francis Co., 2008.
[22] P. Lin, P.L.-F. Liu, A numerical study of breaking waves in the surf zone, J. Fluid Mech. 359 (1998) 239–264.
[23] P. Lin, C.-W. Li, A σ-coordinate 3-D numerical model for surface wave propagation, Int. J. Numer. Method Fluid 38 (2002) 1045–1068.
[24] P. Lin, C.-W. Li, Wave–current interaction with a vertical square cylinder, Ocean Eng. 30 (2003) 855–876.
[25] P. Lin, C. Man, A staggered numerical algorithm for the extended Boussinesq equations, Appl. Math. Model. 31 (2007) 349–368.
[26] D. Liu, Numerical modeling of three-dimensional water waves and their interaction with structures, Ph.D. thesis, National University of Singapore, 2007.
[27] T. Nakayama, K. Washizu, Nonlinear analysis of liquid motion in a container subjected to forced pitching oscillation, Int. J. Numer. Method Eng. 15 (1980) 1207–1220.
[28] T. Nakayama, K. Washizu, The boundary element method applied to the analysis of two-dimensional nonlinear sloshing problems, Int. J. Numer. Method Eng. 17 (1981) 1631–1646.

[29] T. Okamoto, M. Kawahara, Two-dimensional sloshing analysis by Lagrangian finite element method, Int. J. Numer. Method Fluid 11 (1990) 453–477.
[30] T. Okamoto, M. Kawahara, 3-D sloshing analysis by an arbitrary Lagrangian–Eulerian finite element method, Int. J. Comput. Fluid Dyn. 8 (1997) 129–146.
[31] W.J. Rider, D.B. Kothe, Reconstructing volume tracking, J. Comput. Phys. 141 (1998) 112–152.
[32] J. Smagorinsky, General circulation experiments with the primitive equations, Mon. Weather Rev. 91 (1963) 99–164.
[33] C.Z. Wang, B.C. Khoo, Finite element analysis of two-dimensional nonlinear sloshing problems in random excitations, Ocean Eng. 32 (2005) 107–133.
[34] G. Wei, J.T. Kirby, Time-dependent numerical code for extended Boussinesq equations, J. Waterw. Port Coast. Ocean Eng.-ASCE 121 (1995) 251–261.
[35] G.X. Wu, Q.A. Ma, R.E. Taylor, Numerical simulation of sloshing waves in a 3D tank based on a finite element method, Appl. Ocean Res. 20 (1998) 337–355.
[36] G.X. Wu, R.E. Taylor, D.M. Greaves, The effect of viscosity on the transient free-surface waves in a two-dimensional tank, J. Eng. Math. 40 (2001) 77–90.
[37] H.G. Verhagen, L. Wijingaarden, Non-linear oscillation of fluid in a container, J. Fluid Mech. 22 (1965) 737–751.
[38] H.A. Van der Vorst, Iterative Krylov Methods for Large Linear Systems, Cambridge University Press, New York, USA, 2003.